Supporting Information

Photochemical Design of Stimuli Responsive Nanoparticles Prepared by Supramolecular Host-Guest Chemistry

*Astrid F. Hirschbiel,[1,2] Bernhard V. K. J. Schmidt,[3] Peter Krolla-Sidenstein,[4] James P. Blinco,[5] Christopher Barner-Kowollik[1,2,5]**

[1]Preparative Macromolecular Chemistry, Institut für Technische Chemie und Polymerchemie (ITCP), Karlsruhe Institute of Technology (KIT), Engesserstr. 18, 76128 Karlsruhe, Germany.

[2]Soft Matter Synthesis Laboratory, Institute for Biological Interfaces (IBG), Karlsruhe Institute of Technology (KIT), Hermann-von-Helmholtz-Platz 1, 76344 Eggenstein-Leopoldshafen, Germany.

[3]Max Planck Institute of Colloids and Interfaces, 14424 Potsdam, Germany.

[4]Institute of Functional Interfaces (IFG), Karlsruhe Institute of Technology (KIT), Hermann-von-Helmholtz-Platz 1, 76344 Eggenstein-Leopoldshafen, Germany.

[5]School of Chemistry, Physics and Mechanical Engineering, Queensland University of Technology (QUT), 2 George St, 4001 Brisbane, Queensland, Australia.

*To whom correspondence should be addressed

E-mail: *christopher.barner-kowollik@kit.edu*

Characterization of the synthesised compounds

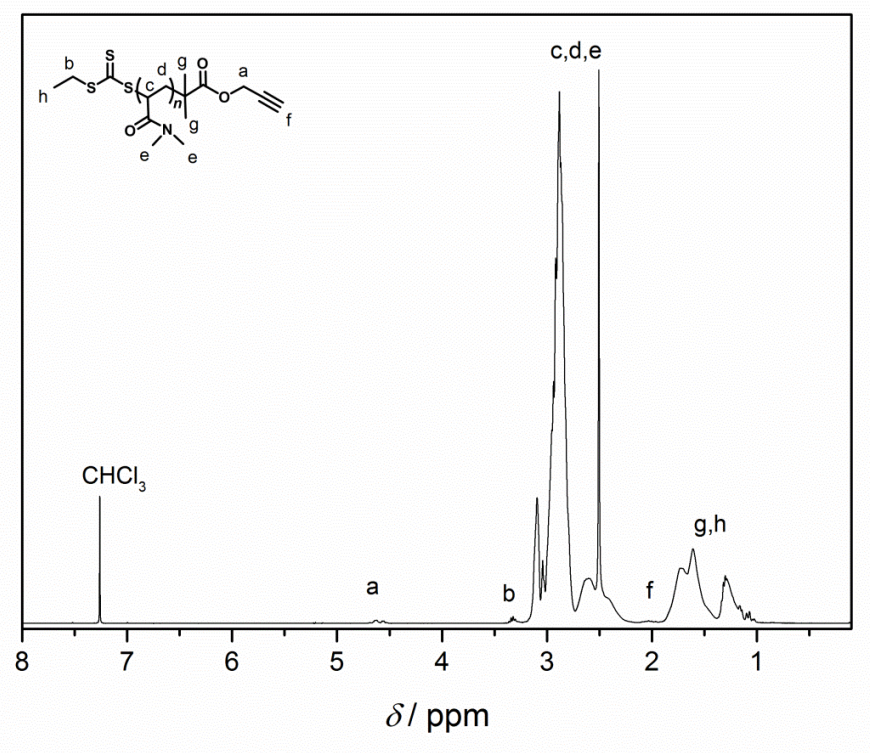

Figure S1. ^{1}H NMR (400 MHz, $CDCl_3$) of poly(DMAAm)-alkyne (**2**).

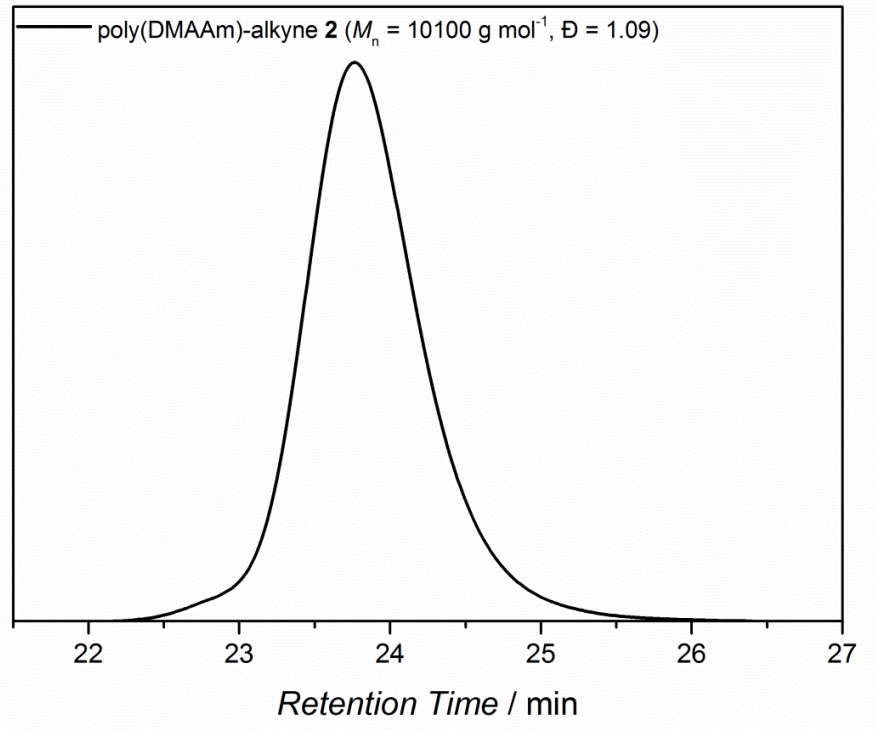

Figure S2. SEC trace of poly(DMAAm)-alkyne (**2**) measured in DMAC at 50 °C.

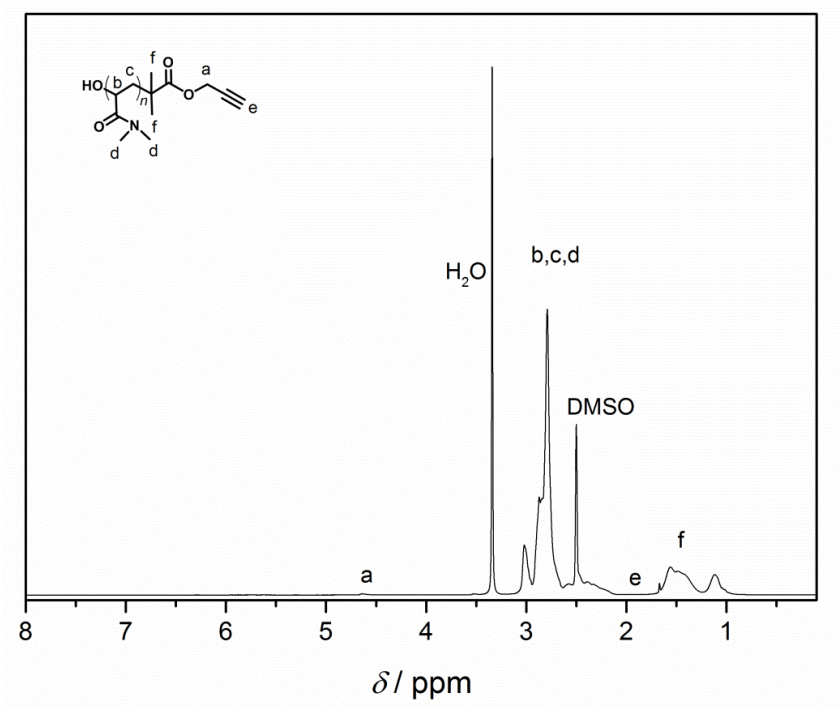

Figure S3. ^{1}H NMR (400 MHz, DMSO-d_6) of alkyne-poly(DMAAm)-OH (**3**).

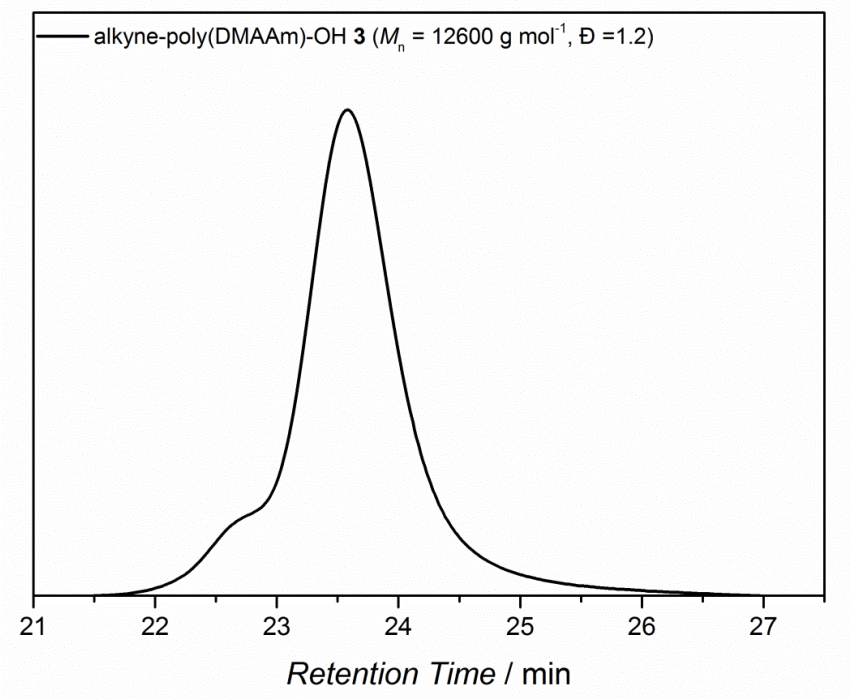

Figure S4. SEC trace of alkyne-poly(DMAAm)-OH (**3**) measured in DMAC at 50 °C.

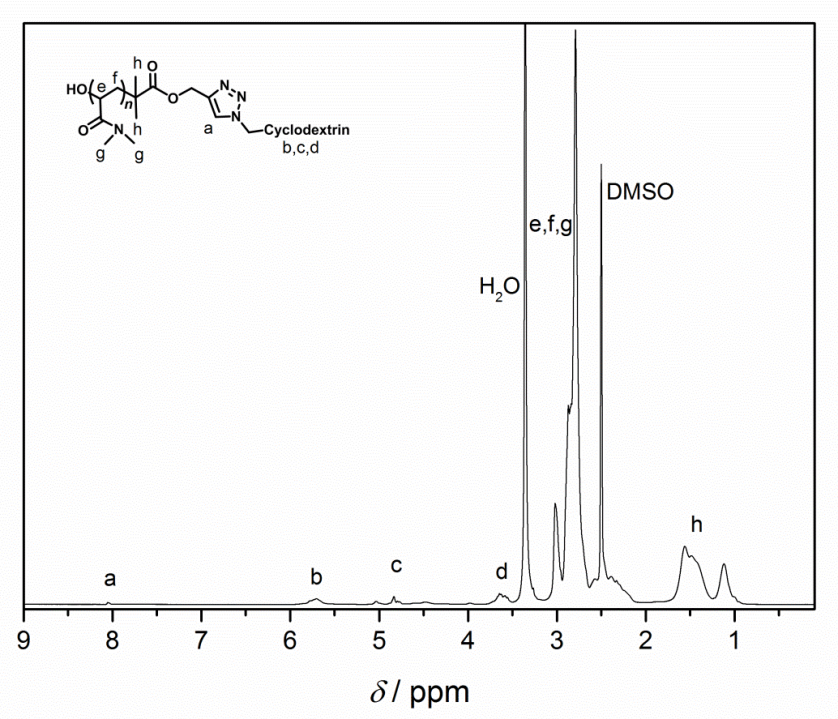

Figure S5. ^{1}H NMR (400 MHz, DMSO-d_6) of poly(DMAAm)-β-CD (**5**).

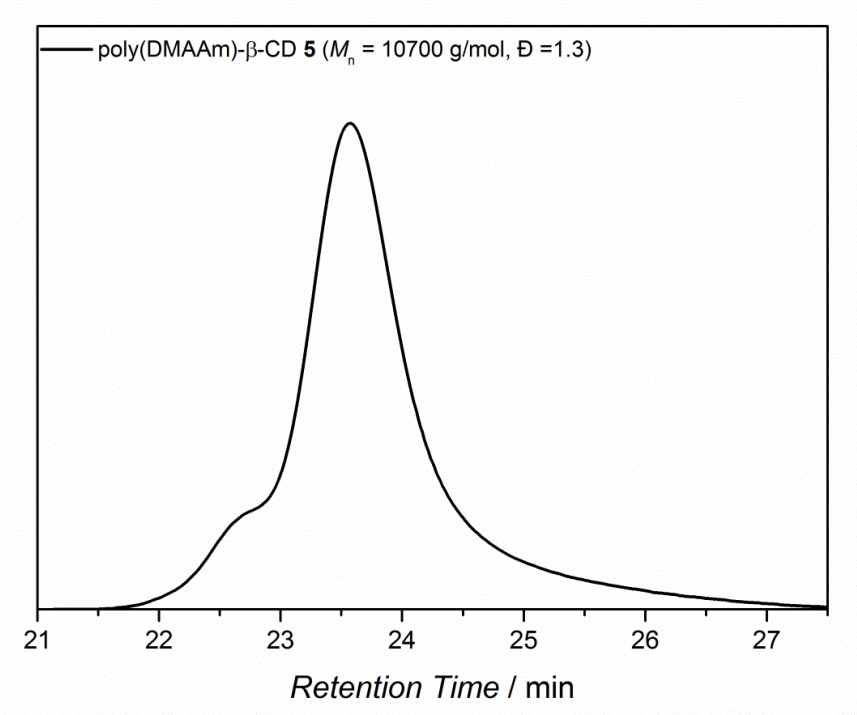

Figure S6. SEC trace of poly(DMAAm)-β-CD (**5**) measured in DMAC at 50 °C.

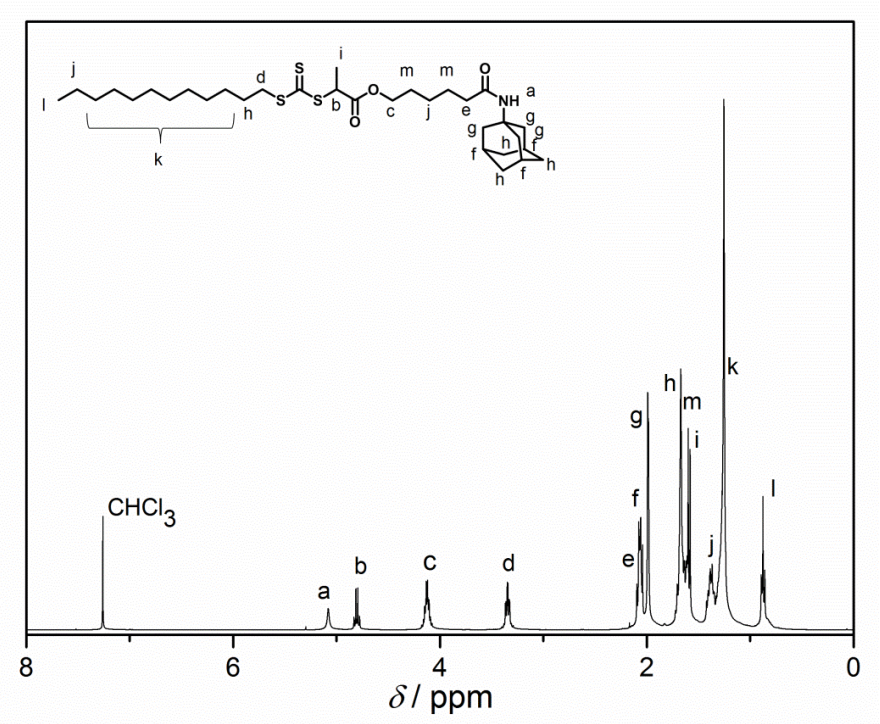

Figure S7. ^{1}H NMR (400 MHz, $CDCl_3$) of 6-(((3s,5s,7s)-adamantan-1-yl) amino)-6-oxohexyl 2-(((dodecylthio) carbonothioyl) thio) propanoate (**8**).

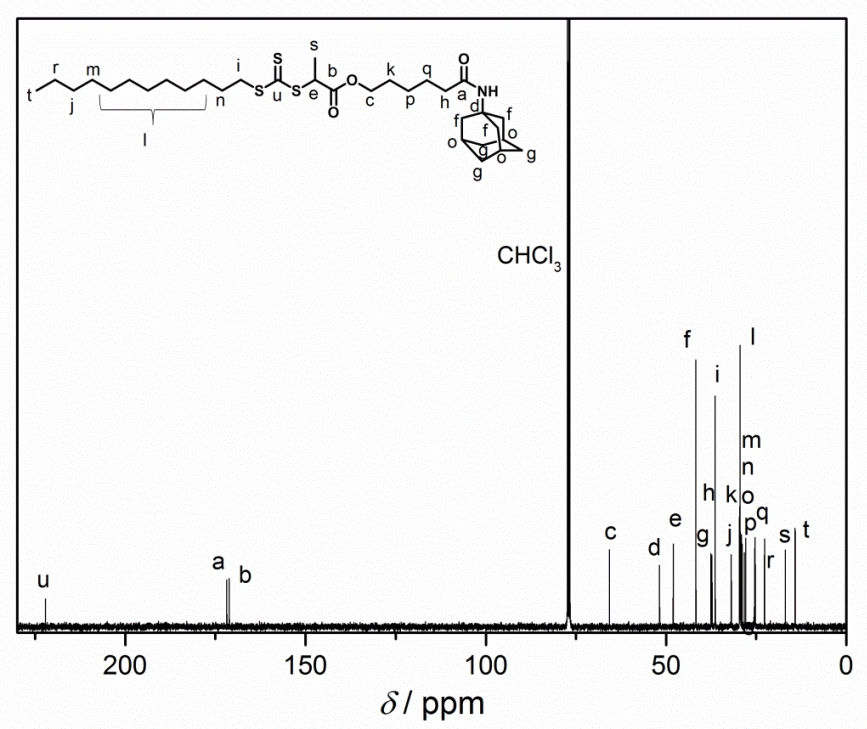

Figure S8. ^{13}C NMR (400 MHz, $CDCl_3$) of 6-(((3s,5s,7s)-adamantan-1-yl) amino)-6-oxohexyl 2-(((dodecylthio) carbonothioyl) thio) propanoate (**8**).

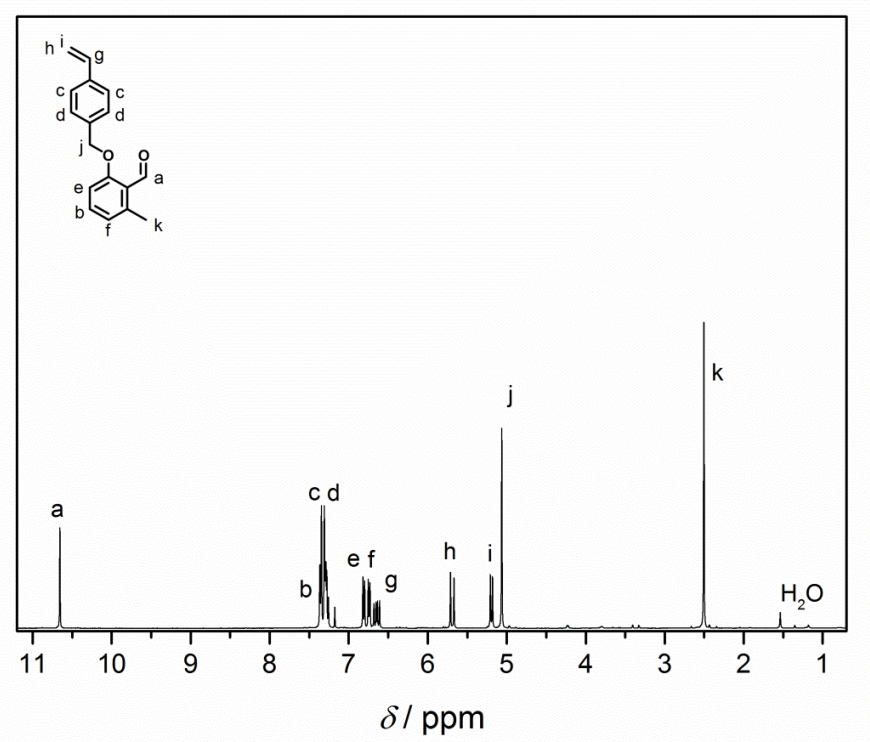

Figure S9. ^{1}H NMR (400 MHz, $CDCl_3$) of 2-methyl-6-((4-vinylbenzyl)oxy)benzaldehyde (**9**).

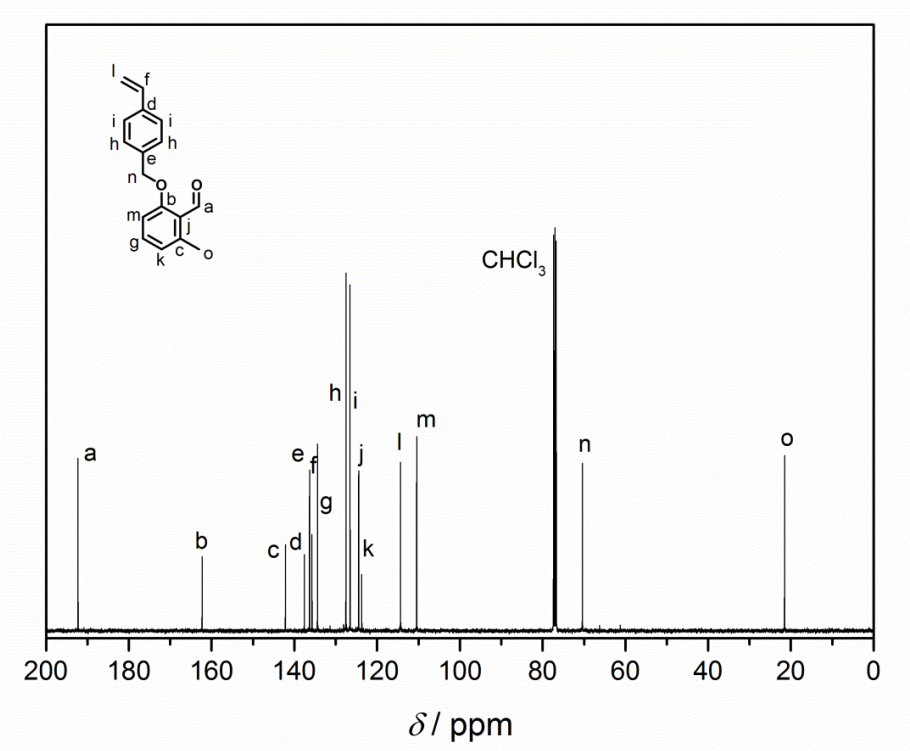

Figure S10. ^{13}C NMR (400 MHz, $CDCl_3$) of 2-methyl-6-((4-vinylbenzyl)oxy)benzaldehyde (**9**).

Kinetic Study

A kinetic study of the RAFT polymerization of methyl acrylate (Figure S11) and *N*-isopropylacrylamide (Figure S12) mediated by 6-(((3s,5s,7s)-adamantan-1-yl) amino)-6-oxohexyl 2-(((dodecylthio) carbonothioyl) thio) propanoate (DoPAT-Ada) (**8**) was carried out. The conversion of poly(MA) was determined gravimetrically. Therefore, the reaction mixture was aliquoted into separate vials in a glove box after three consecutive freeze pump thaw cycles, and subsequently placed in a heating block at 60 °C. Samples were drawn from the reaction mixture at preset time intervals, quenched and weighed. After the evaporation of the monomer, the samples were weighed again and conversion was determined. In addition, the conversion of poly(NiPAAm) was deduced from the corresponding NMR spectra by integration of the vinyl proton resonances against the polymer backbone resonances, which decrease with increasing conversion. In both cases the experimental molecular weight ($M_{n\ exp}$) was obtained from size exclusion chromatography. $M_{n\ exp}$ was plotted against conversion to evidence the linear behavior of the molecular weight evolution. Additionally, ESI-mass spectra were recorded after precipitation of selected polymer samples. The spectra in Figure S11 show a clean RAFT controlled polymer distribution with no further side products. The reactions conditions for the two reactions can be found in Table S1 and Table S2.

Table S1. Reaction conditions for the DoPAT-Ada **8** mediated polymerization of methyl acrylate in toluene as well as the calculated number average molecular weight based on 100% conversion ($M_{n\ theo}$). c^0_{Mon} is the concentration of the monomer, c^0_{CTA} is the concentration of DoPAT-Ada and c^0_{AIBN} is the initial AIBN concentration.

c^0_{Mon} [mmol L^{-1}]	c^0_{CTA} [mmol L^{-1}]	c^0_{AIBN} [mmol L^{-1}]	T [°C]	$M_{n\ theo}$ [g mol^{-1}]
5530.95	24.29	2.38	60	20000

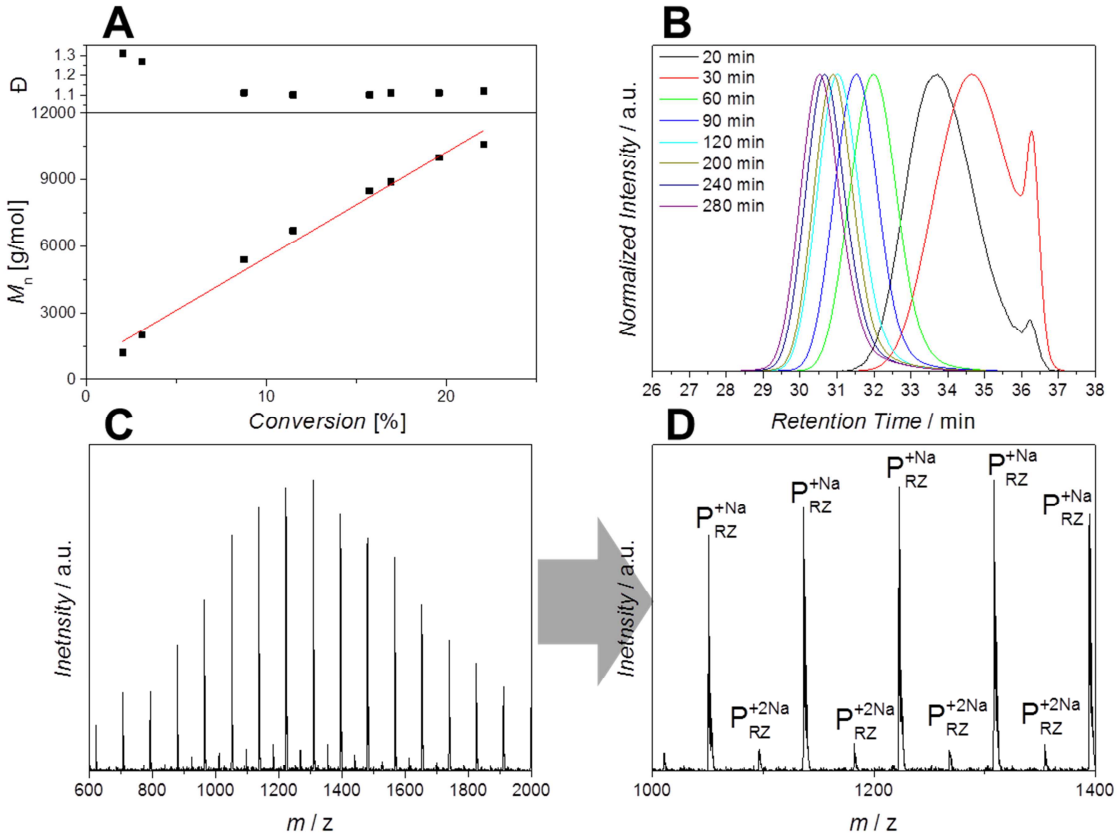

Figure S11. Kinetic study of CTA **8** with methyl acrylate DP_n = 200. A) M_n (relative to PS standards with the Mark Houwink parameters of poly(MA)) and $Đ$ versus conversion. B) SEC traces in THF at 35 °C. C) ESI-MS spectrum. D) Magnification of the ESI-MS spectrum.

Table S2. Reaction conditions for the DoPAT-Ada **8** mediated polymerization of *N*-isopropylacrylamide in 1,4-dioxane as well as the calculated number average molecular weight based on 100% conversion ($M_{n\ theo}$). c^0_{Mon} is the concentration of the monomer, c^0_{CTA} is the concentration of DoPAT-Ada and c^0_{AIBN} is the initial AIBN concentration.

c^0_{Mon} [mmol L^{-1}]	c^0_{CTA} [mmol L^{-1}]	c^0_{AIBN} [mmol L^{-1}]	T [°C]	$M_{n\ theo}$ [g mol^{-1}]
1841.05	86.73	8.67	60	3000

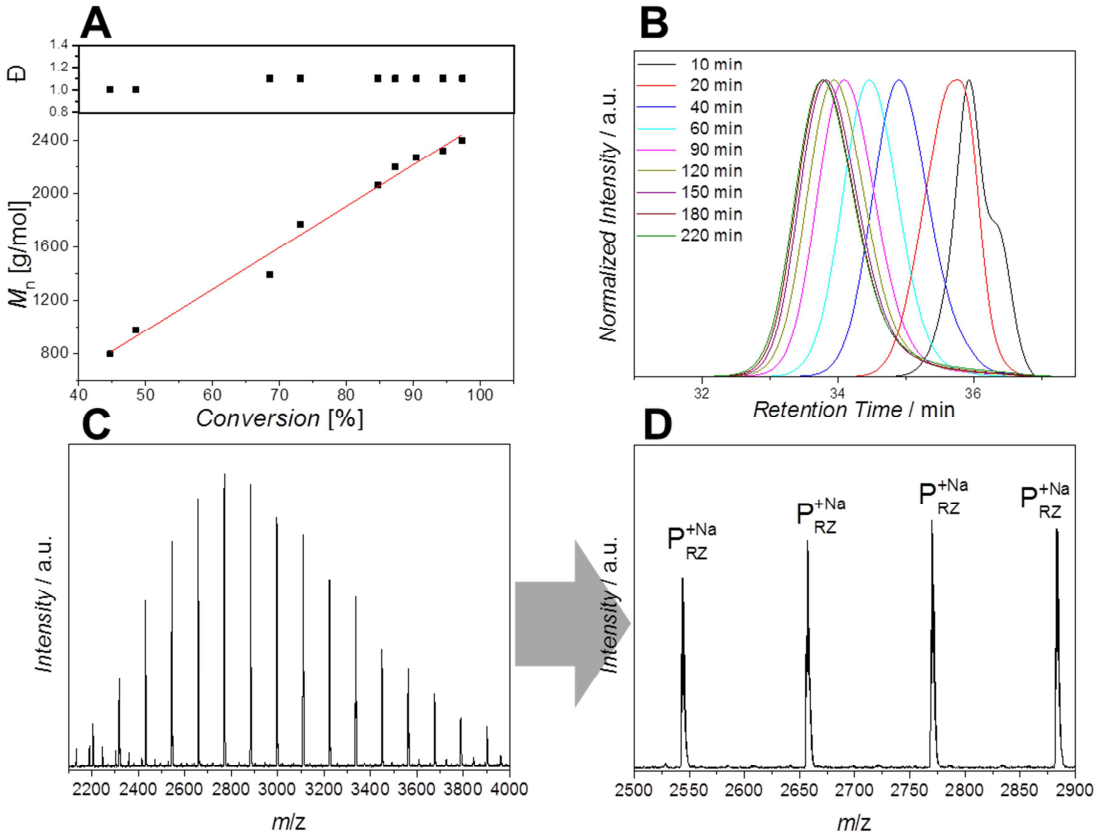

Figure S12. Kinetic study of CTA **8** with *N*-isopropylacrylamide (DP_n = 27). A) M_n (relative to PS standards with the Mark Houwink parameters of poly(NIPAAm)) and *Đ* versus conversion. B) SEC traces in THF at 35 °C. C) ESI-MS spectrum. D) Magnification of the ESI-MS spectrum.

Chain Extension

Chain extension was performed with the macro-CTA obtained in the RAFT co-polymerization of NiPAAm and the photoenol monomer **9**. The chain extension confirms the living character of the polymerization.

Table S3. Reaction conditions for the chain extension of poly(NiPAAm/PE)-Ada with *N*,*N*-dimethylacrylamide in 1,4-dioxane as well as the calculated number average molecular weight based on 100% conversion ($M_{n\ theo}$). c^0_{Mon} is the concentration of the monomer, c^0_{CTA} is the concentration of DoPAT-Ada and c^0_{AIBN} is the initial AIBN concentration.

c^0_{Mon} [mmol L^{-1}]	c^0_{CTA} [mmol L^{-1}]	c^0_{AIBN} [mmol L^{-1}]	T [°C]	$M_{n\ theo}$ [g mol^{-1}]
470.26	2.33	0.23	67	40000

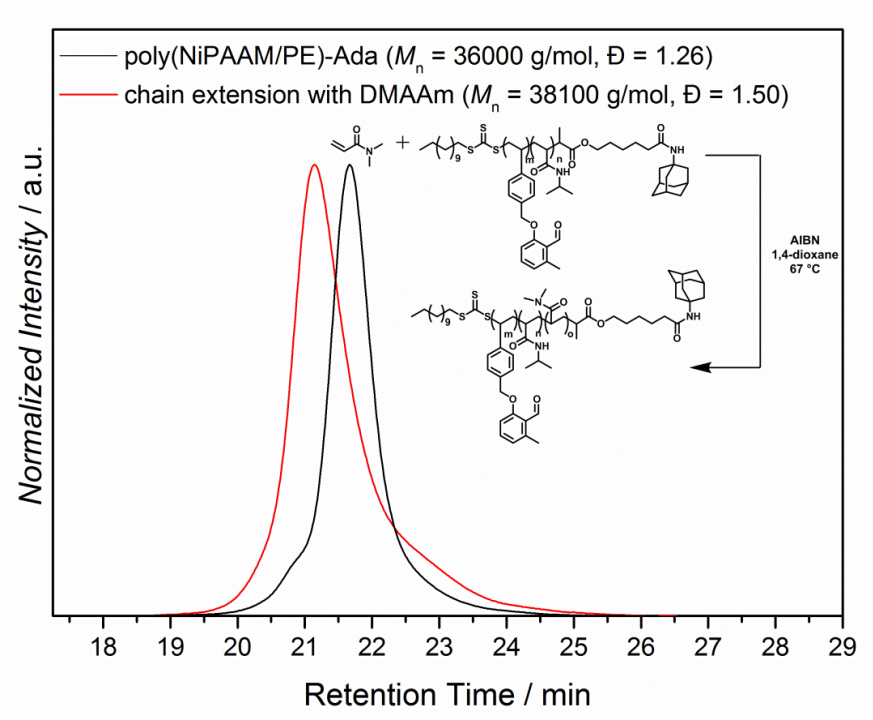

Figure S13. SEC trace of poly(NiPAAm/PE)-Ada before and after chain extension with *N*,*N*-dimethylacrylamide. The samples were measured in DMAC at 50 °C relative to PS standards.

Calculation of the theoretical molecular weight

The theoretical molecular weights were calculated with the following equation:

$$M_{n\,theo} = \left(\frac{[monomer]}{[CTA]_0} \times M_{monomer} \times U\right) + M_{CTA}$$

Autocorrelation functions of the DLS measurements

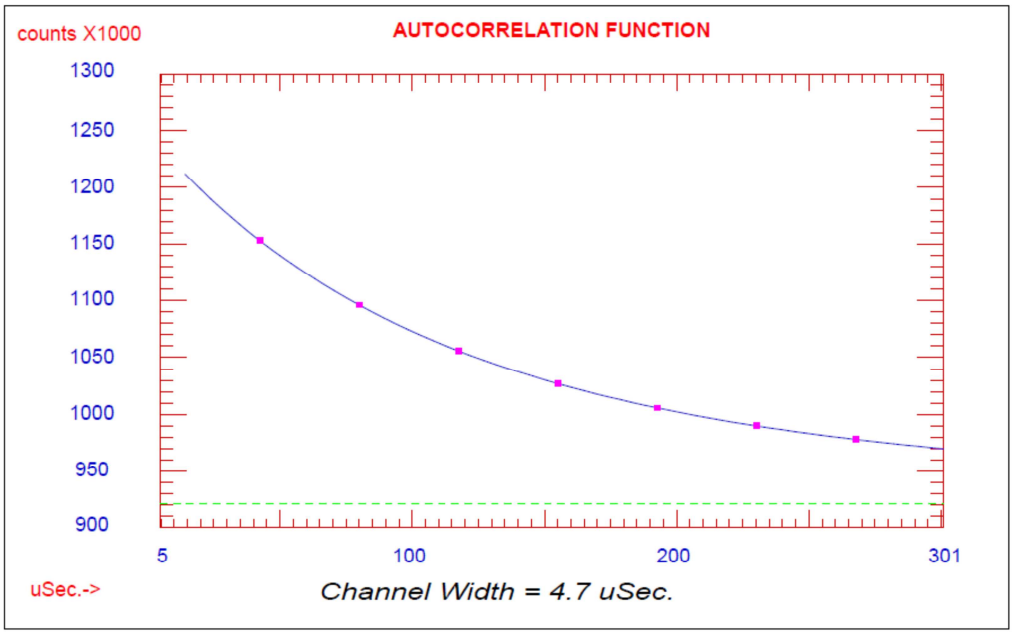

Figure S14. Autocorrelation function of the DLS measurement of poly(NiPAAm/PE)-Ada **10**.

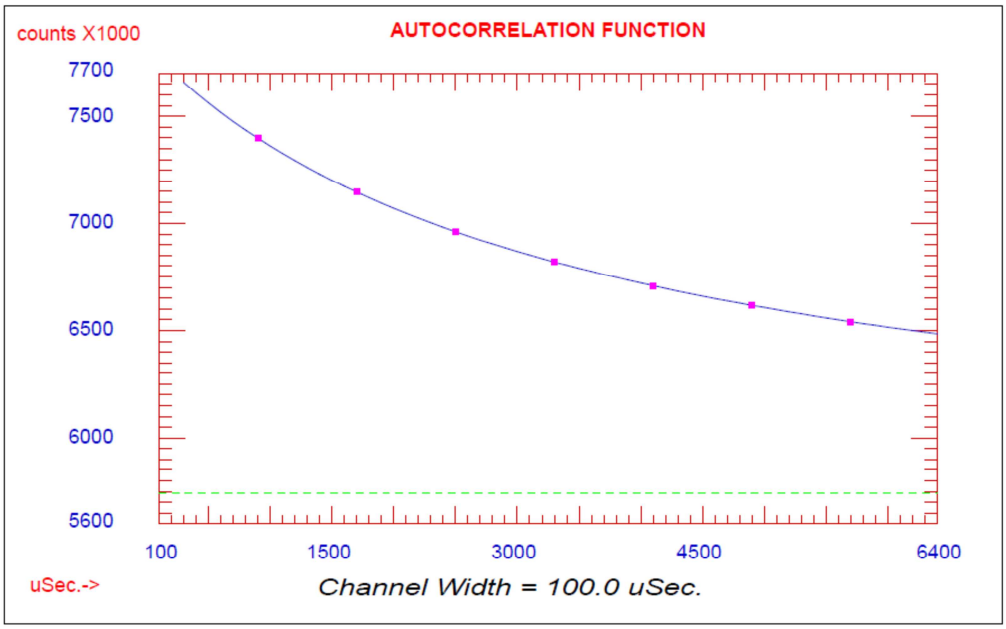

Figure S15. Autocorrelation function of the DLS measurement of poly(DMAAm)-β-CD **5**.

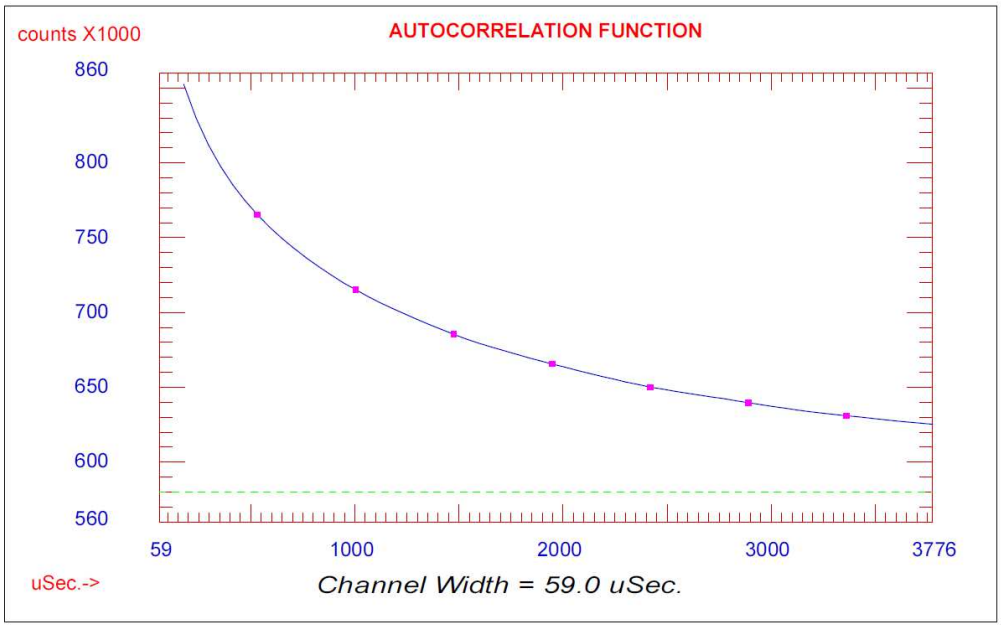

Figure S16. Autocorrelation function of the DLS measurement of the supramolecular diblock copolymer **11**.

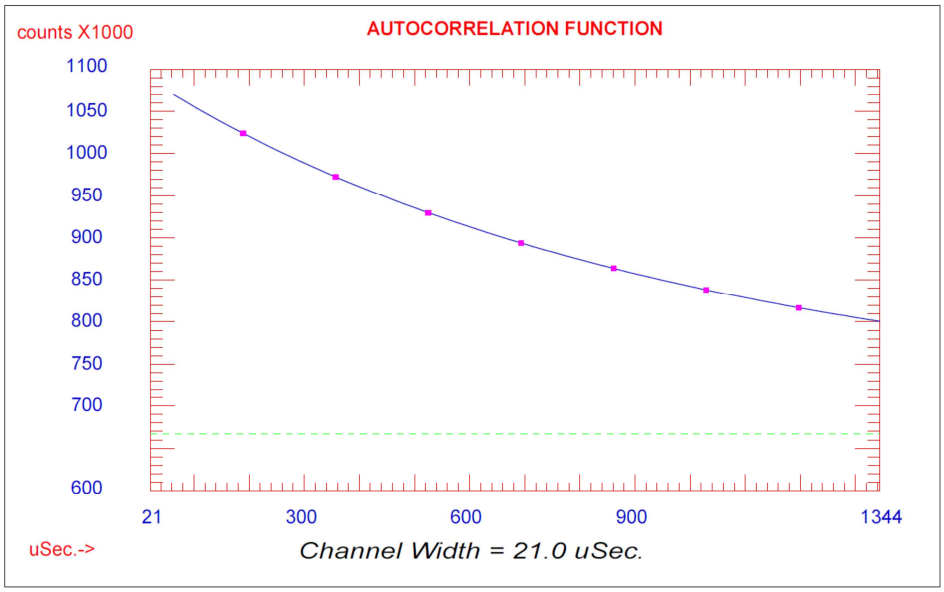

Figure S17. Autocorrelation function of the DLS measurement of the polymeric micelle **13**.

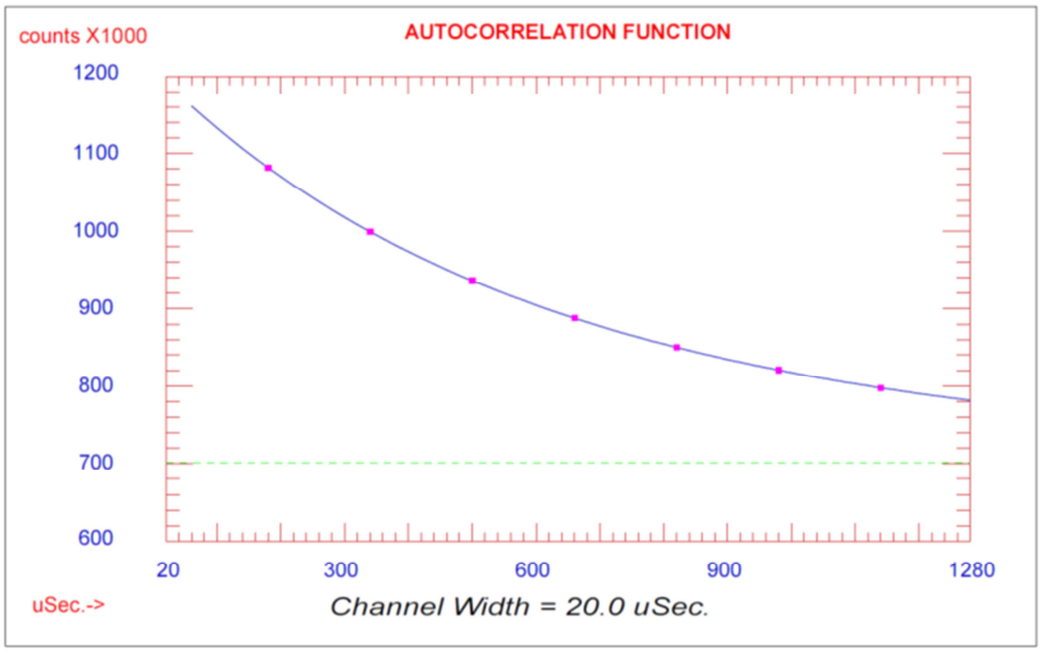

Figure S18. Autocorrelation function of the DLS measurement of the nanoparticle **14**.

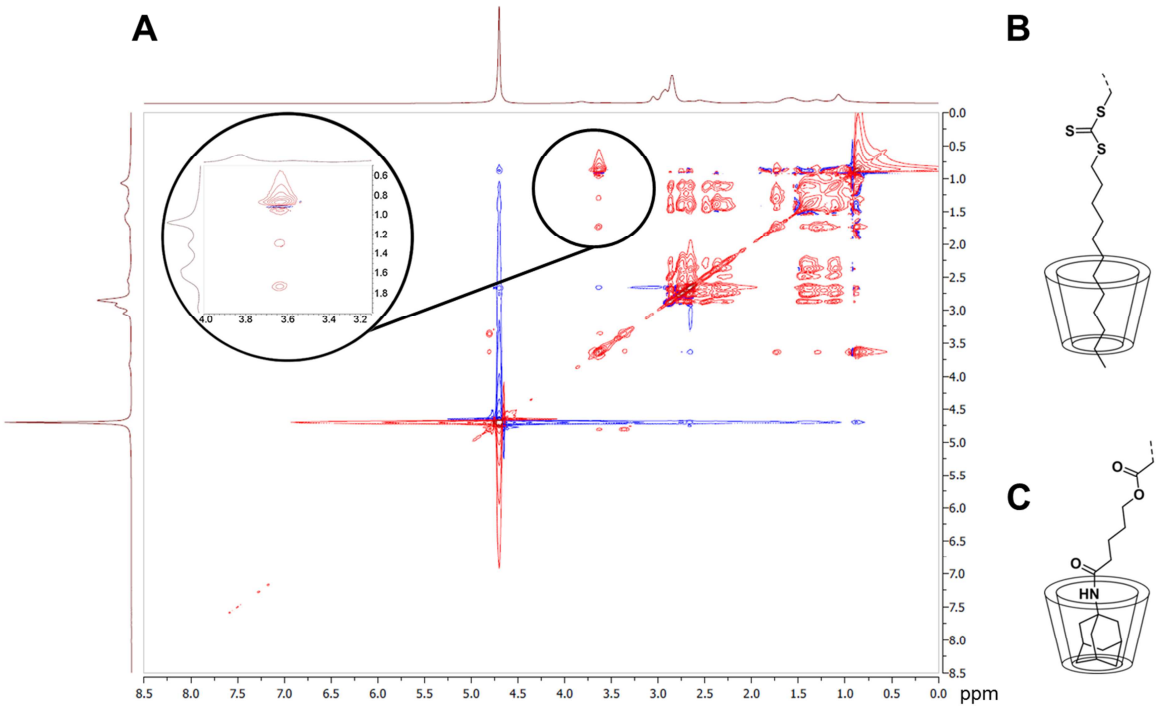

Figure S19. A) 2D NOESY NMR spectrum of the supramolecular diblock copolymer 11 in D_2O at 10 °C. The cross-correlation peaks evidencing the close proximity of the inner protons of β-CD and the adamantyl protons are highlighted in the spectrum. B) Structure of the inclusion complex of β-CD and the alkyne chain of the DoPAT unit, whose cross-correlation peaks also appear in the circled area. C) Structure of the inclusion complex of β-CD and the adamantyl unit of poly(NiPAAm/PE).

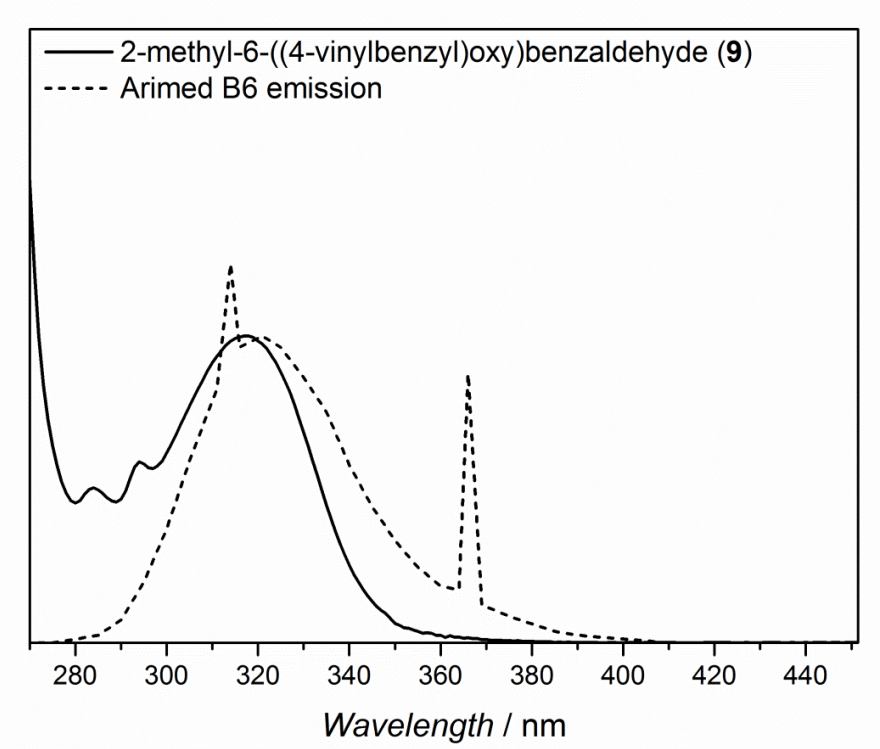

Figure S20. Emission spectrum of the employed compact low-pressure fluorescent lamp (Arimed B6, 36W) and the UV-Vis spectrum of 2-methyl-6-((4-vinylbenzyl)oxy)benzaldehyde (**9**) measured in acetonitrile.

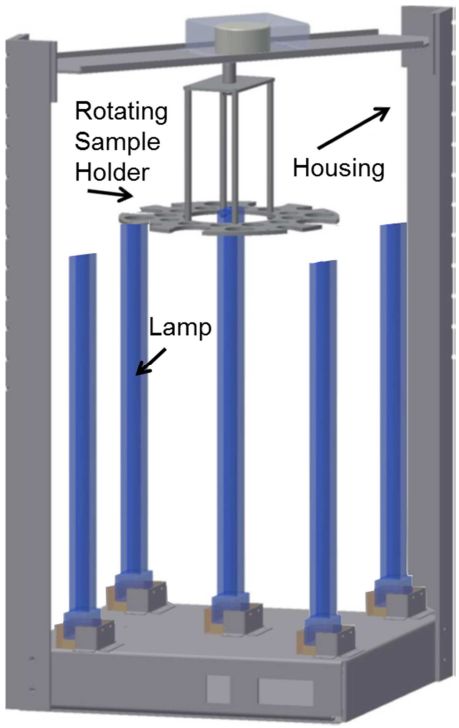

Figure S21. Illustration of the custom-built photo-reactor employed in the current study.

^{1}H NMR spectra: Cleavage of micelle arms and subsequent centrifugation.

AFM particle analysis

Particles analysis was performed from freshly cleaved mica surfaces with NanoScope Analysis 1.40 (Bruker). The detected particles are colored in light blue. The spots colored in dark blue are agglomerates in the sample and were not considered in the analysis. Figure S23 illustrates the 2D topographic image of the micelles along with the statistical data collected in a table, and a histogram of the particle diameters. The same analysis was performed for the nanoparticle sample and is depicted in Figure S24. In general, a decrease in diameter on average from micelles to nanoparticles is observed.

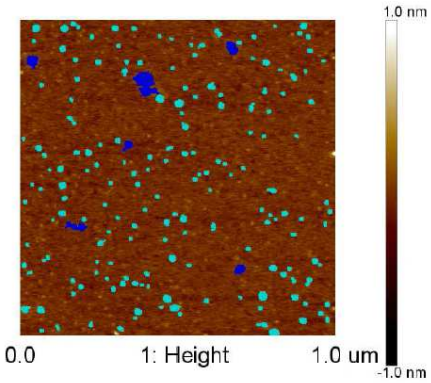

Parameter	Mean	Minimum	Maximum	Sigma
Total Count	172.000	172.000	172.000	0.000
Density	172.000 (/µm^2)	172.000 (/µm^2)	172.000 (/µm^2)	0.000 (/nm^2)
Height	340.758 (pm)	51.629 (pm)	1212.988 (pm)	259.087 (pm)
Area	217.704 (nm^2)	95.367 (nm^2)	583.649 (nm^2)	114.977 (nm^2)
Diameter	16.143 (nm)	11.019 (nm)	27.260 (nm)	4.072 (nm)

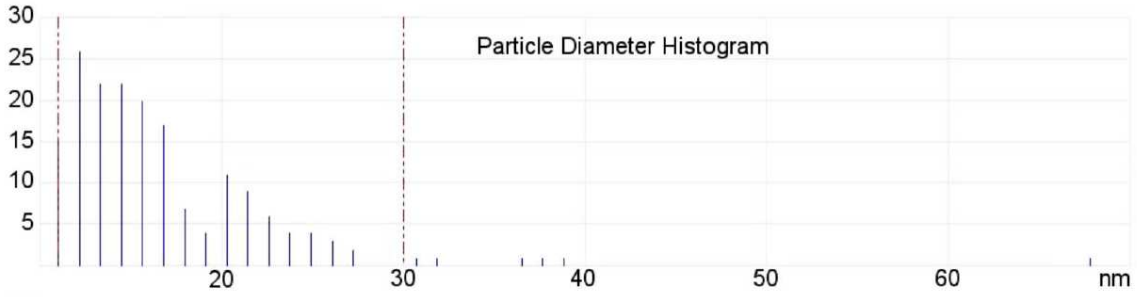

Figure S22. AFM particles analysis of the micelle sample.

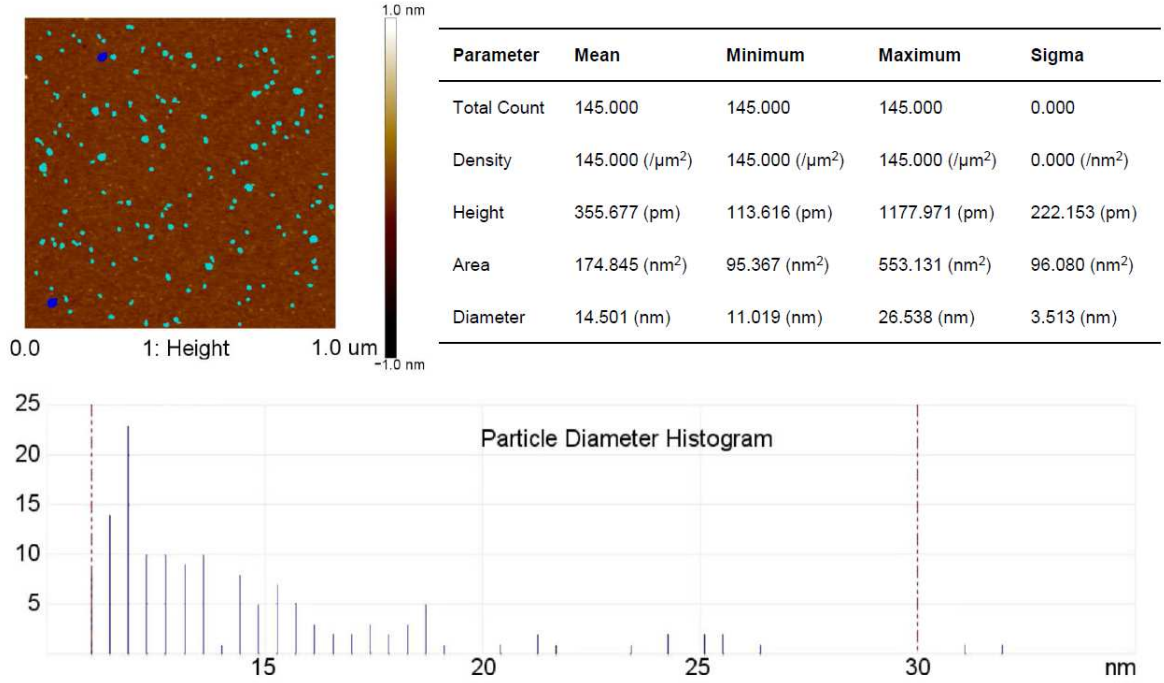

Parameter	Mean	Minimum	Maximum	Sigma
Total Count	145.000	145.000	145.000	0.000
Density	145.000 (/µm^2)	145.000 (/µm^2)	145.000 (/µm^2)	0.000 (/nm^2)
Height	355.677 (pm)	113.616 (pm)	1177.971 (pm)	222.153 (pm)
Area	174.845 (nm^2)	95.367 (nm^2)	553.131 (nm^2)	96.080 (nm^2)
Diameter	14.501 (nm)	11.019 (nm)	26.538 (nm)	3.513 (nm)

Figure S23. AFM particle analysis of the nanoparticle sample.

Higher magnification AFM images

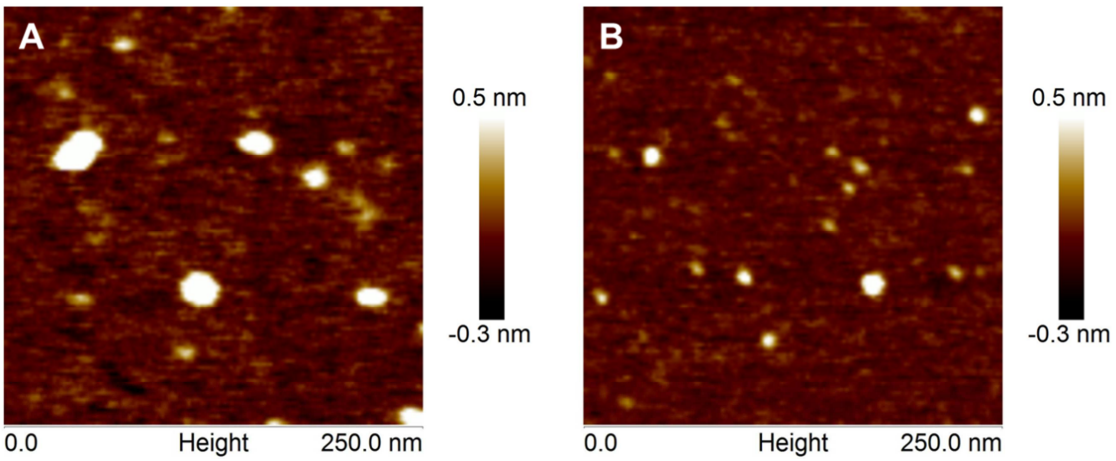

Figure S24. Higher magnification AFM images of A) micelles (**13**) and B) nanoparticles (**14**).